Virtual Pivot Point MEMS Rotary Comb Actuator with Externally Mounted Mirror for Optical Applications

T. M. Fahim Amin[*], M. Q. Huda[**], J. Tulip[***] and Wolfgang Jäger[****]

[*]Dept. of Electrical and Computer Engineering and Dept. of Chemistry, University of Alberta, Edmonton, AB T6G 2V4, Canada, tmfahim@ualberta.ca
[**]Dept. of Chemistry, University of Alberta, Edmonton, AB T6G 2G2, mqhuda@ualberta.ca
[***]Boreal Laser Inc., Edmonton, AB T5L 2H7, jtulip@telus.net
[****]Dept. of Chemistry, University of Alberta, Edmonton, AB T6G 2G2, wolfgang.jaeger@ualberta.ca

ABSTRACT

In this paper, we present the design, fabrication, and characterization of a virtual pivot point micro electromechanical systems (MEMS) electrostatic actuator with externally mounted mirror. The point of rotation of the actuator's movable arm is distant from the physical actuator, which is a requirement for certain applications, such as an external cavity laser in Littman configuration. The dynamic characterization of the device with a finite element analysis simulation shows that the resonance frequency of the in-plane rotational mode is well separated from that of the out-of-plane bending mode, confirming high in-plane stability. The devices were fabricated on a silicon-on-insulator wafer with device layer thickness of 100 µm. Thin mirrors were fabricated by dicing a 100 µm thick silicon wafer. A resonance frequency of about 5.9×10^2 Hz for the maximum sized mirror (1.7 mm x 100 µm x 1.0 mm) was determined by optical characterization.

Keywords: MEMS, optical MEMS, external cavity laser, tunable laser, micromirror.

1 INTRODUCTION

MEMS mirrors have become very popular micro fabricated devices because of their usefulness in many applications. While some of these applications are already at the commercial stage, such as projection displays, optical scanners, and optical switching [1-3], significant research activities are currently directed towards the use of MEMS mirrors in other applications, including external cavity lasers (ECLs) [4], adaptive optics [5], optical tomography [6, 7], and galvanometric scanners [8]. In many cases, the anticipated application dictates the size of the MEMS mirror and its plane of movement. Micro-sized mirrors favor high frequency operation which is suitable in switching and projection display operation. Many other applications demand larger mirror sizes to achieve sufficient light reflection for its operation [5-9]. Most of the large MEMS mirrors reported in the literature are fabricated on top of the silicon plane and provide out-of-plane movement through a tilt motion. However, some applications, for example mirror tuning of an ECL, demand in-plane lateral movement of the MEMS component. MEMS devices can be fabricated for lateral operation using bulk micromaching processes of silicon-on-insulator (SOI) wafers. However, the size of the mirror is limited by the thickness of the device layer and the maximum achievable uniform etching depth. The surface quality of the etched sidewall is also an issue for applications that require minimum light scattering. One way to overcome this issue is to mount an external mirror onto a MEMS actuator [10]. In our previous work, we discussed the design of a virtual pivot point (VPP) actuator for application in Littman configured ECLs [11]. The mirror size in the previous design was limited by the device layer thickness of the SOI wafer.

In this paper, we present the design and fabrication process of a VPP actuator with the provision of mounting external optical components. The VPP actuator has a maximum radius of up to 5 mm and a physical clearance of 3 mm from the pivot point location. We also describe an efficient process for mounting an externally fabricated mirror onto the MEMS actuator.

2 DEVICE STRUCTURE AND OPERATION

Continuous wavelength tuning of an ECL in both Littrow and Littman configuration is possible through rotation of the tuning element (mirror/grating) about a pivot point [12]. The VPP actuator described here is specifically designed for operation in a Littman configured ECL, in which optical beam and rotation axis intersect. The VPP of the actuator allows the laser beam to pass through and provides space for optical components. Nevertheless, the actuator can equally be used in Littrow configured ECLs and other optical applications which require large mirrors. The device has a maximum radius of 5 mm and a physical clearance of 3 mm from the pivot point. A schematic diagram of the designed VPP rotary comb electrostatic actuator is shown in Fig. 1. Four sets of rotary comb drive pairs were used in the design to generate sufficient

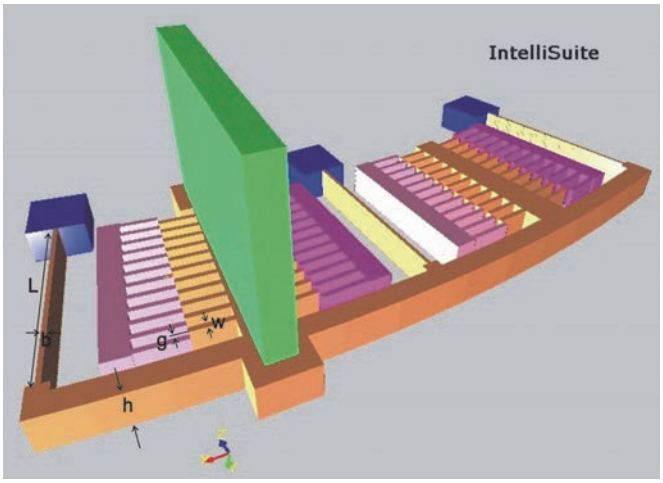

Figure 1: A schematic diagram of a VPP actuator with mounted external mirror.

electrostatic force for the desired rotation. The comb drives are connected through rigid arc-shaped trusses at the top and the entire movable structure is anchored through three beams. Two trusses from which the moving comb fingers extend are positioned along the radial direction from the VPP. They were designed with high stiffness to carry the mirror. See Table 1 for design parameters.

The electrostatic force generated by a set of *n* rotary comb fingers with an applied voltage V is given by:

$$F = \frac{n\varepsilon h V^2}{g} \qquad (1)$$

Here, h is the finger thickness, g is the gap between the fingers, ε is permittivity of air, and n is the number of moving comb fingers. In our design, two of the four sets of comb drives generate force to rotate the actuator in one direction (for example, the first and third comb drives for clockwise rotation) and the other two actuate during rotation in the opposite direction. The electrostatic force is balanced by the restoring spring force provided by the three anchored beams according to Hooke's law. We simulated the structure using the MEMS simulation software Intellisuite to obtain the actuator displacement as a function of applied voltage. The displacement of the structure at the topmost point in x-direction versus voltage is shown in Figure 2 (solid black line). The behaviour of the structure was also simulated to determine the effect of mounting an external mirror. The resonance frequency of structure decreases with increase of mirror mass, as anticipated. The two dashed traces in Fig. 2 show the change of resonance frequency with mirror mass. Mode 1 represents the in-plane vibration and mode 2 the out-of-plane vibration of the structure. It is apparent that the frequency of the out-of-plane vibration frequency is much higher than the in-plane frequency, which confirms the in-plane stability of the structure.

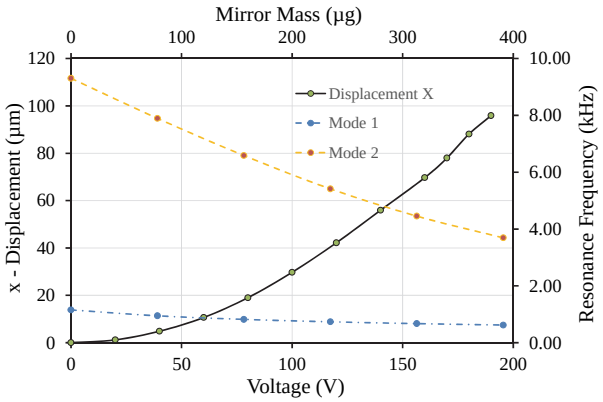

Figure 2: Displacement at the topmost point of the actuator along the x-coordinate as function of voltage (solid line) and variation of the resonance frequencies of the actuator (lowest two modes) with mirror mass.

	Length/Arc size	**Width**	**Height**
Beam Dimension	1500 µm	9 µm	100 µm
Comb Finger	3.7 deg	7.4 µm	100 µm
Mirror Size	1.7 mm	100 µm	1 mm
Maximum Radius from Pivot Point	5010 µm		

Table 1: Design parameters of the fabricated actuator.

3 DEVICE FABRICATION

The actual device has dimensions of 2 mm x 2 mm and was fabricated on a 4 mm x 5 mm chip. An SOI wafer with device layer thickness of 100 µm, buried oxide layer of 2 µm, and substrate layer thickness of 300 µm, as depicted in Fig. 3 (a)-(j), was used for the device fabrication. Bulk micro-machining was performed from both sides of the wafer, involving two level masking. The mask sets were designed with largely spaced open areas around the devices to facilitate easier mounting of the external mirror and easier alignment of the light beam onto the mirror. This made the fabrication process quite challenging as the wafer weakened from the huge backside Si removal. We developed a fabrication process that involves patterning of both sides of the wafer before any deep etch. At first, a thermal oxide layer was grown on both sides of the wafer as masking layer to utilize the higher etching selectivity of SiO_2 over Si (100:1). Aluminum (Al) was then deposited on the backside of the wafer with a sputtering process to assist the alignment of front and back patterns. The Al layer on the backside was then patterned by photolithography using HPR 506 photoresist followed by etching with commercial Al etchant (16:1:1:2 solution of phosphoric acid, nitric acid, acetic acid, and water).

The pattern was then transferred onto the oxide layer by etching the SiO_2 layer using a reactive ion etch (RIE) process. The same process, except the Al patterning steps, was used to pattern the front side SiO_2 layer. The backside

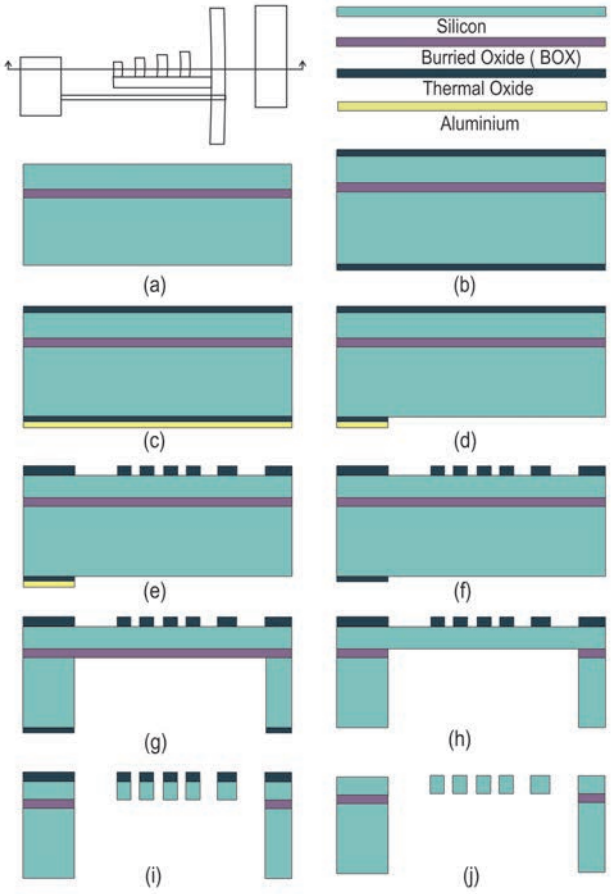

Figure 3: Step-by-step illustration of actuator fabrication; (a) SOI Wafer; (b) thermally grown oxide on both sides; (c) Al sputtering on back side; (d) patterning of Al, etching Al layer and oxide layer; (e) patterning of front layer; (f) removal of Al from back; (g) removal of Si using DRIE; (h) removal of buried oxide; (i) etching of Si device layer and (j) removal of residual thermal oxide from top.

Al layer, opaque to infrared light, assisted the alingnment process without any deep etch. After this stage, the wafer was diced into individual dies for further processing. Batches of 10 to 20 dies were then mounted on a carrier wafer and deep etching of Si down to the buried oxide layer was performed from the back side. An optimized deep RIE (DRIE) recipe was used in an STS inductively coupled plasma (ICP) machine to achieve good vertical feature profiles. Subsequently, we removed the buried oxide layer using RIE from the back side. The dies were then un-mounted from the carrier wafer and thoroughly cleaned. We mounted them again on a carrier wafer and performed DRIE from the front side to transfer the pattern onto the Si device layer from the oxide mask. The actuators were released upon completion of this stage. The residual oxide mask layer was then removed using RIE and a thin gold layer was deposited using a sputtering process for better electrical contact. An SEM image of a fabricated device is shown in Fig. 4.

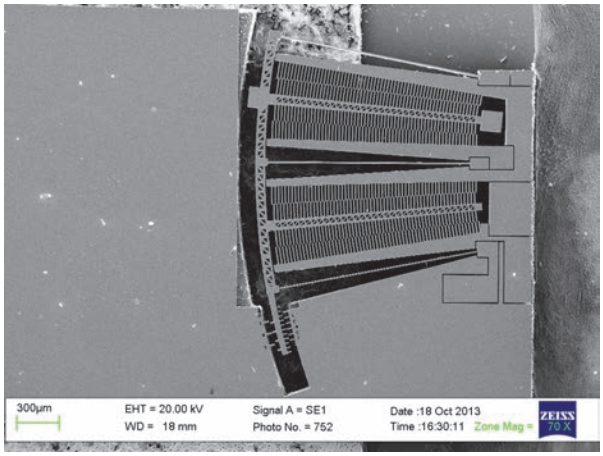

Figure 4: An SEM image of a VPP actuator.

4 EXTERNAL MIRROR MOUNTING

Two contact pads were inscribed at the top and bottom of the right truss in our design to facilitate mounting of an external mirror, as shown in Fig. 4. Si mirrors were fabricated from a commercially available 100 µm thin Si wafer, polished on both sides. The wafer was first diced into different suitable mirror sizes using a Disco DAD 321 dicing saw. Thin layers of chromium (Cr ~ 15 nm) and gold (Au ~ 50 nm) were then deposited onto the individual mirror pieces through sputtering. Gold was used on the mirror surface to increase its reflectivity. We developed an efficient method to mount the external mirror onto the MEMS device to minimize problems associated with manual handling of the thin Si mirrors. A die bonding system consisting of a microscope, a moving stage, a heater, and a vacuum tip, was used to develop the miror mounting method. Epotek H20E Silver filled epoxy was used as the bonding material between the MEMS device and the mirror. The epoxy can be cured by keeping at 120^0 C for 15 minutes. The mirror mounting setup is shown in Fig. 5. The die bonding system (Fig. 5(a)) has different types of vacuum tips just above the movable stage. An enlarged view of the tip assembly is shown by the arrow. We used the second tip from the left. The needle was used to pick up a drop of epoxy and the vacuum tip (next to it), which has a slot to keep the mirror straight, was used to pick up the mirror piece and to release it. Fig. 5(b)-(c) shows the epoxy mixture and a tiny dot of epoxy on the needle. A mirror picked up vertically by the vacuum tip is shown in Fig. 5(d). The mirror piece was aligned with the mirror holder on the MEMS actuator and released onto it with the help of the microscope and moving arm. Fig. 5(e) shows an SEM image of an actuator with mounted external mirror.

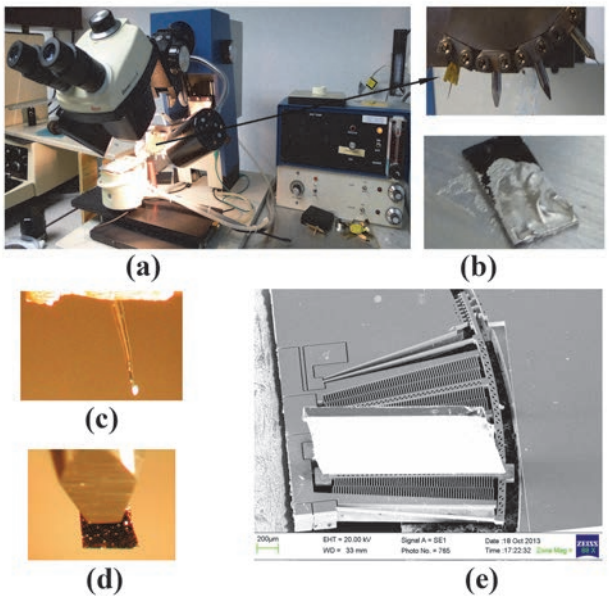

Figure 5: Mirror mounting setup and mounting process; (a) the die bonding machine used for mirror mounting (the top right picture shows a close-up of the vacuum tips); (b) silver epoxy mixture; (c) a drop of epoxy at the tip of the needle; (d) a mirror picked up by the vacuum tip; and (e) an SEM image of an actuator with mounted mirror.

5 RESULTS AND DISCUSSION

A vernier scale was inscribed into each chip during the mask design to facilitate measurement of the rotation angle on a wafer probing station. Measured and simulated rotation angles are in excellent agreement (see Fig. 6). We also achieved symmetrical displacements in clockwise and counter-clockwise directions. After mounting the mirror, we characterized the device using optical techniques. The beam of a red laser pointer was aimed at the mounted mirror and the reflected beam was detected using a photodector. The photodector output was recorded with a digital oscilloscope. The device was actuated with a square wave driving voltage and the vibration after the sudden actuation was captured. Analysis of the oscilloscope traces resulted in a lowest vibration frequency of 5.9×10^2 Hz for a maximum mounted mirror size of 1.7 mm x 100 µm x 1 mm. This is very close to simulated frequency of 6.2×10^2 Hz. The slight deviation can be attributed to uneven beam widths of the actuator produced in the DRIE process.

6 CONCLUSIONS

In this paper, we presented the design and fabrication of a VPP comb- drive actuator with the provision of mounting optical components. The dynamic characterization of the actuator confirms the in-plane stability of the devices with mounted external mirror. A procedure for mounting optical components was developed. An optical characterization of the device confirms its resonance frequency to be 5.9×10^2 Hz for a mounted mirror size of 1.7 mm x 100 µm x 1 mm.

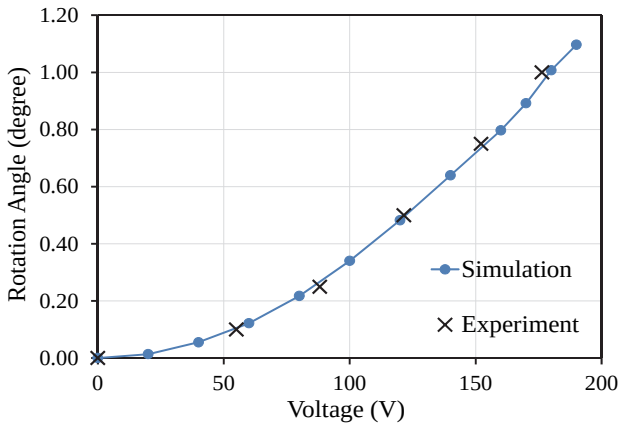

Figure 6: Measured and simulated rotation angles of the actuator as function of applied voltage.

ACKNOWLEDGEMENTS

We thank Dr. G. McKinnon and Dr. N. Ponnampalam, Norcada Inc., for discussions and support, and for help with the development of the mirror mounting technique. This work was supported by the nanoWorks Program of Alberta Innovates Technology Futures and by the Natural Sciences and Engineering Research Council of Canada.

REFERENCES

[1] P. F. van Kessel, L. J. Hornbeck, R. E. Meier and M. R. Douglass, P IEEE, 86, 1687, 1998.
[2] N. Asada, M. Takeuchi, V. Vaganov, N. Belov and I. Sluchak, Sensor Actuat. A-Phys., 83, 284, 2000.
[3] P. De Dobbelaere, K. Falta, S. Gloeckner and S. Patra, Commun. Magazine, IEEE, 40, 88, 2002.
[4] A. Q. Liu and X. M. Zhang, J. Micromech. Microeng., 17, R1, 2007.
[5] P.-Y. Lin, H.-T. Hsieh and G.-D. J. Su, J. Opt., 13, 055404, 2011.
[6] Y. Pan, H. Xie and G. K. Fedder, Opt. Lett., 26, 1966, 2001.
[7] B. Qi, A. P. Himmer, L. M. Gordon, X. D. V. Yang, L. D. Dickensheets and I. A. Vitkin, Opt. Commun., 232, 123, 2004.
[8] L. O. S. Ferreira and S. Moehlecke, Sensor Actuat. A-Phys., 73, 252, 1999.
[9] T. Fujita, K. Maenaka and Y. Takayama, Sensor Actuat. A-Phys., 121, 16, 2005.
[10] J. D. Berger, Y. Zhang, J. D. Grade, H. Lee, S. Hrinya and H. Jerman, Optical Fiber Communication Conference and Exhibit, OFC 2001, TuJ2-TuJ2, 2001.
[11] T. Amin, M. Huda, Y. Ning, G. McKinnon, J. Tulip and W. Jäger, Proc. SPIE, 84900D, 2012.
[12] M. G. Littman and H. J. Metcalf, Appl. Opt., 17, 2224, 1978.